Electron-impact-induced oxidation of Al(111) in water vapor: Relation to the Cabrera-Mott mechanism

H. D. Ebinger and J. T. Yates, Jr.
Department of Chemistry, Surface Science Center, University of Pittsburgh, Pittsburgh, Pennsylvania 15260
(Received 13 May 1997)

The oxidation of an Al(111) single-crystal surface induced by 100 eV electron bombardment in water vapor at room temperature has been studied using x-ray photoemission spectroscopy and electron-energy-loss spectroscopy. Electron bombardment significantly increases the growth rate and changes the observed growth-rate law in comparison to the oxidation without the electron beam. The aluminum oxide film grows with linear rather than parabolic time-dependent kinetics up to a thickness of about 25 Å. After reaching this thickness, the growth rate slows down significantly. During oxidation the oxide film becomes electrically charged on its surface and the normal electric field in the oxide remains constant. The results are discussed in the framework of a Cabrera–Mott type oxidation mechanism. [S0163-1829(98)01303-4]

I. INTRODUCTION

The substrate temperature is of major importance for surface oxidation since dissociation of the oxidizing agent, surface diffusion, and ion migration are thermally activated processes. Therefore, the growth rate and the thickness of an oxide film increase with increasing temperature, while the number of defects shows the inverse behavior. This principle holds for the oxidation of both semiconductors and metals. In semiconductor device technology there is, therefore, a high interest in growing oxide films using nonthermal excitation pathways. Such pathways include electron-induced and photon-induced oxidation processes. Nonthermal activation for oxidation is of interest for metals as well, in order to possibly improve the corrosion resistance and protection of the metal substrate.

Energy to overcome activation barriers might be supplied in a number of ways, one of which is the electron bombardment of the surface covered with an oxidizing agent. It is well known that electron bombardment leads to the dissociation of water molecules by electronic excitation.[1,2] Recently a study using a water film on top of a hydrogen-covered silicon surface showed that oxidation induced by electron impact occurs at cryogenic temperatures.[3] The dissociation of the water molecule can be achieved by electron energies as low as 6 eV.[3] The cross section for water conversion is high, making electron impact activation an effective route for surface oxidation. This bears a close relation to other experiments in which the oxidation of an oxygen-covered surface is induced by the tunneling current between the surface and the tip of a scanning-tunneling microscope (STM) instrument.[4] Both studies clearly show the feasibility of electron stimulated surface oxidation.

The bombardment of a water-ice layer on an Al(111) surface with low-energy electrons converts water into surface oxide as well.[5] By working at 90 K this process could be clearly separated from thermally activated surface oxidation. As in the case of silicon, we found a high cross section (2.5×10^{-16} cm^2, 100 eV electrons) for electron-induced oxidation.[5] This cross section is several orders of magnitude above the cross section for the destructive interaction of electrons with aluminum oxide itself.[6,7] The oxide layer formed under electron bombardment of water on Al(111) is an amorphous precursor of bulk Al_2O_3.[5]

In this work, we extend our previous measurements at 90 K (Ref. 5) to 300 K in order to probe the effectiveness of electron-induced oxidation of Al(111) under practical conditions.

II. EXPERIMENT

The experimental ultrahigh vacuum apparatus (base pressure$=2\times10^{-10}$ Torr) has been described in detail previously.[8] Briefly, it is a multichamber system permitting transfer of the Al(111) crystal from a high-pressure dosing and electron-impact chamber to an analytical section containing a hemispherical electron spectrometer for XPS and electron-energy-loss spectroscopy (EELS) measurements. Al $K\alpha$ x-ray irradiation is used for XPS measurements. Further analytical instrumentation, which has not been applied in this study, includes a microchannelplate low-energy electron diffraction (LEED) apparatus, a shielded quadrupole mass spectrometer, calibrated and collimated gas dosers, and a high-resolution electron-energy-loss (HREEL) spectrometer.

Calibration of the binding-energy scale for the electron spectrometer is made using clean Al and Au surfaces and binding-energy values from Ref. 11. Absolute binding-energy values are accurate to within ±0.2 eV. However, the relative differences between peak energies can be determined with much better precision by the help of a fitting procedure. The spectrometer was operated at a pass energy of 150 eV for XPS and 30 eV for the EEL spectra. The takeoff angle for XPS between the surface normal and the electron spectrometer is 35° unless otherwise stated.

Two different Al(111) crystals have been employed in this study with diameters of 15 and 12 mm. The first one has been cut, oriented, and polished in our laboratory while the second one was obtained from MaTeck, Jülich. Both were oriented to within 0.25 degrees of the (111) direction and polished to a mirror finish. The crystal was mounted between two *W* support wires by means of a slot in the crystal edge. Heating was done resistively by passing current through the

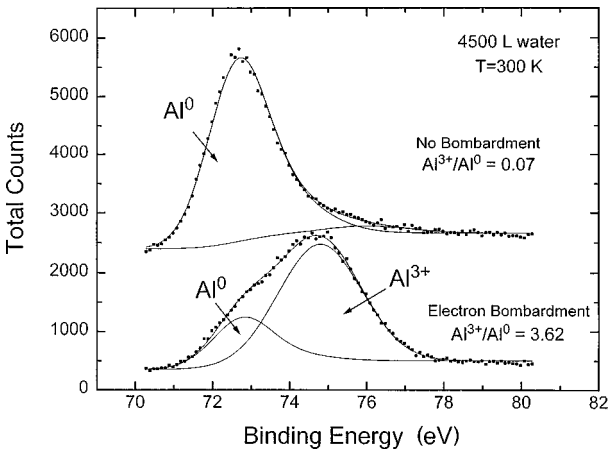

FIG. 1. Al($2p$) core-level emission after comparable water exposures with and without 10 μA/cm^2 electron bombardment (100 eV). In the upper spectrum without electron bombardment only a slight change on the high-binding-energy side of the bulk Al^0 contribution corresponding to oxide formation is visible. The lines are the result of the peak fitting procedure (see text). The lower spectrum involving electron bombardment shows a dominant Al^{3+} signal from aluminum oxide. The peak area ratios are noted in the figure.

support wires (up to 25 A). The surface was cleaned by 1 kV Ar^+ bombardment at 400 K and annealed at 670–730 K until all impurities were reduced to limiting levels. The temperature is measured by a type-K thermocouple.

The oxide growth experiments were done in the high-pressure cell of the system with the crystal mounted on a liquid-nitrogen cooled manipulator and maintained at 300 K by electrical heating using a feedback controller connected to the thermocouple. Water vapor was supplied by backfilling through a leak valve. For electron bombardment, a broad-beam electron gun (indirectly heated BaO cathode) giving a uniform flux over the entire crystal surface was employed.[12] The pressure gauge was arranged in order to have the crystal facing away from the hot ion gauge filament during electron bombardment. All experiments have been done in a water background pressure of 5×10^{-7} Torr (H_2O exposures are quoted in Langmuirs L where $1\,L=1\times10^{-6}$ Torr s, uncorrected for ion gauge sensitivity), and under 100 ev electron bombardment with a current density of 10 μA/cm^2. This corresponds to a deposited power of only 1 mW/cm^2, and will cause negligible crystal heating. We observe no change in the crystal temperature reading when switching on the electron beam.

III. RESULTS

A. Increased oxidation rate using electron-beam-assisted excitation

Figure 1 shows a comparison of the Al($2p$) core-level region for comparable water exposures with and without electron bombardment. The oxidation of the aluminum surface can be followed by the growth of an $Al^{3+}(2p)$ core-level component at about 75 eV binding energy.[13–15] The area of this peak is proportional to the coverage of aluminum oxide on the surface in the low coverage regime. The upper spectrum has been measured after 4500 L of water vapor exposure with the crystal at 300 K. Only slight oxidation can be seen from the change in signal at 75 eV binding energy. In the lower spectrum we show the Al($2p$) core-level emission after the same treatment but with 10 μA/cm^2 electron bombardment (100 eV) during exposure. Electron bombardment leads to a much more intense Al^{3+} component corresponding to increased surface oxidation.

Peak intensities of the Al($2p$) and the O($1s$) signal have been obtained by fitting Gaussian functions to the spectra and calculating the peak area. The energy dependence of the background intensity, $b(E)$, due to inelastic scattering has been taken into account[16] by assuming that spectral features $s(E')$ at higher kinetic energies E' contribute with a certain weight constant k to the signal as shown in Eq. (1):

$$b(E)=b_0+k\int_E^\infty s(E')dE'. \tag{1}$$

The offset parameter b_0 is the counting rate at the high-kinetic-energy end of the selected energy range. Assuming Gaussian-like core-level signals, $s(E)$, the integral gives the error function erf(E). The constant k typically is 0.03, which means that the background increases typically by 3% going from the high- to the low-energy side of a loss peak.

The result of the peak fitting procedure is shown in Fig. 1 (solid lines). The Al($2p$) core-level region can be described by the Al^0 signal from the metal substrate and the Al^{3+} signal from the oxide film. Since the Al^0 peak shows a long tail towards the high-binding-energy side, we used the sum of two Gaussian functions to model it. The relative intensity, energy position, and half-width has been kept constant for these two peaks, the peak area being the only parameter changing during electron-induced oxidation. For spectra in which oxidation has occurred, an Al^{3+} contribution appears in the spectra that can be described by one Gaussian function with varying peak area, binding energy, and half-width. The same holds for the O($1s$) oxygen core-level emission to be shown later. The Al^{3+}/Al^0 peak area ratios obtained from the fitting procedure are noted in Fig. 1.

The intensity of the Al^{3+} photoemission feature is small in the case of H_2O adsorption/decomposition without electron bombardment. The O($1s$) intensity is more sensitive for the characterization of oxide film growth than is the $Al^{+3}(2p)$ feature. Figure 2 shows a comparison of the O($1s$) peak areas with and without electron bombardment during water exposure at 300 K. The strong increase in oxygen uptake caused by the electron beam compared to water exposures without the electron beam is clearly visible from the data. While the growth rate continuously decreases with increasing time in water vapor as shown here (Fig. 2) and published,[13,17] the electron bombardment in water vapor leads to a linear oxygen uptake versus time. Comparing the slopes at low water exposures, the oxidation in this case is five times faster when the surface is bombarded with electrons. Both experiments have been done with the crystal in the same position and under the same heating/cooling conditions. A detailed characterization of the oxide film growth during electron bombardment will follow below.

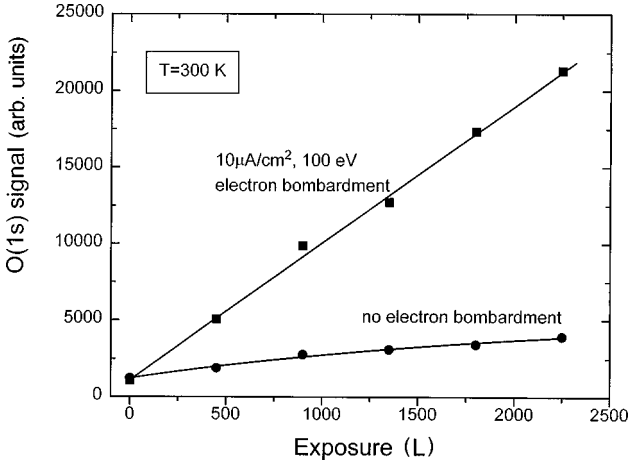

FIG. 2. O(1s) peak area as a function of water exposure. Each step corresponds to 15 min in 5×10^{-7} Torr water. Using continuous electron bombardment (10 μA/cm^2, 100 eV), the rate and level of oxygen uptake can be significantly increased for identical H_2O exposure levels.

B. Film-growth mechanism–electron-beam-assisted oxidation

Figure 3 shows the XPS spectral regions of Al(2p) and O(1s) core-level emission at two stages of film growth for oxide films of 3.5 and 21 Å thickness. All features that are of importance for the characterization of the film-growth process are visible in this plot. The top spectrum has been obtained after 30 min and the bottom spectrum after 195 min of electron beam assisted oxidation. The growth of an aluminum oxide layer is visible from two contributions in the spectrum, the O(1s) oxide peak at about 530 eV and an Al(2p)$^{3+}$ peak at about 75 eV binding energy. Both peaks grow and shift to lower binding energies with increasing film thickness. The increase of the peak intensities with time and the direction and magnitude of the peak shifts are important for understanding the oxide growth mechanism.

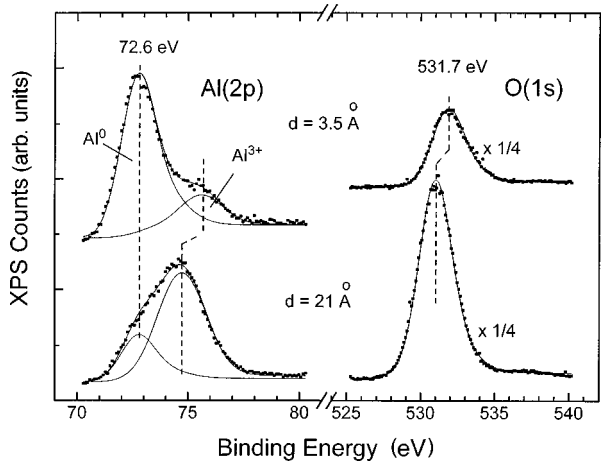

FIG. 3. Al(2p) and O(1s) core-level emission at two different levels of water exposure/electron bombardment. The top spectra correspond to an oxide film thickness of 3.5 Å and the lower spectra to a thickness of 21 Å. Oxidation leads to the buildup of an Al^{3+} peak at about 76 eV binding energy and an oxygen peak at about 531 eV. Both peaks grow in intensity and shift to lower binding energies with increasing oxidation.

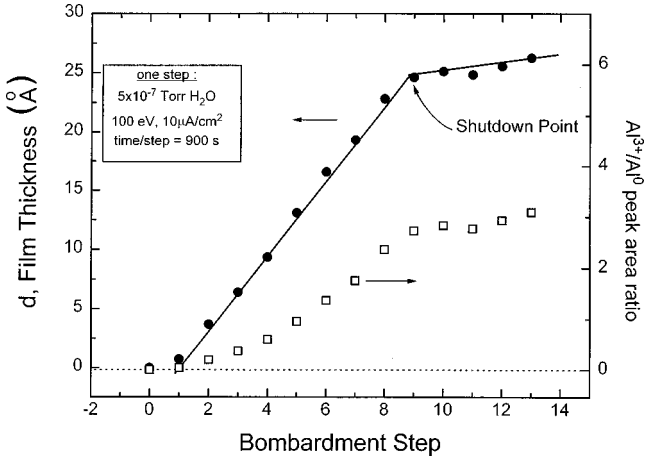

FIG. 4. Film thickness as a function of water exposure/electron bombardment. Each step corresponds to 15 min in 5×10^{-7} Torr water atmosphere, using electron bombardment (10 μA/cm^2, 100 eV). The open squares show the measured Al^{3+}/Al^0 peak area ratio (right ordinate) obtained from peak fitting. The filled circles (left ordinate) show the calculated film thickness assuming a homogeneous oxide layer. As can be seen the thickness increases linearly with bombardment time up to a thickness of about 25 Å. At this point the growth mechanism changes and continuing exposure/bombardment shows a strongly reduced rate.

Figure 4 shows the Al^{3+}/Al^0 peak area ratio (open squares) obtained from peak fitting as a function of surface oxidation. Each step corresponds to 15 min in 5×10^{-7} Torr water vapor using 10 μA/cm^2 (100 eV) electron bombardment. As can be seen by the asymptotic behavior, the oxidation slows down significantly after about eight steps corresponding to 120 min of oxide growth. The same behavior is seen in the plot of the film thickness variation also given in Fig. 4. The thickness has been calculated from the peak area ratio, as will be shown later. The film thickness increases linearly for the first eight oxidation steps and terminates at an oxide film thickness of about 25 Å. This linear increase is quite different from what has been observed for the oxidation in water vapor without electron bombardment (see Fig. 2).[13,17]

Figure 5 shows the shift of the Al^{3+}(2p) and O(1s) peak energies during film growth for the same experiment, as determined from peak fitting. Both peaks undergo a continuous shift to lower binding energies with increasing film thickness. At the limiting thickness of $\sim$25 Å both have shifted by 1 eV. The difference in binding energy between both peaks however remains constant. A similar trend can be observed for the half-width. It increases continuously with film thickness. The solid lines in Fig. 5 follow from a calculation assuming a negative charge on the oxide surface, and taking the potential drop and the final escape depth of the Al(2p) and O(1s) x-ray excited core-level electrons into account.

In Fig. 6 the peak area ratio of the Al^{3+}(2p) and the O(1s) core-level emission is plotted as a function of water exposure/electron bombardment. As can be seen this ratio approaches a saturation value that agrees with the ratio calculated under the assumption of a perfect Al_2O_3 stoichiometry taking the different sensitivities (Leybold-Heraeus compilation) of the electron analyzer for the two emission lines into account. The exposure/bombardment time required for

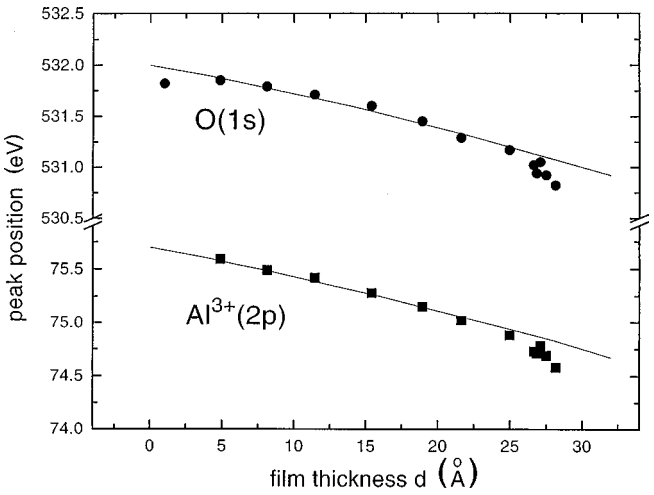

FIG. 5. O1($1s$) and Al^{3+}($2p$) peak position obtained from peak fitting during surface oxidation. Each step corresponds to 15 min in 5×10^{-7} Torr water and electron bombardment (10 μA/cm^2, 100 eV). Both peaks linearly shift in parallel to lower binding energies as the oxide film thickness increases. The behavior can be explained by the formation of O^{2-} ions on the oxide surface.

reaching the saturation value coincides with the shutdown point for of the oxide film growth shown in Figure 4.

C. Characterization of the thick oxide film

1. Film thickness

The characterization of a 25-Å-thick oxide film grown under electron bombardment has been carried out using XPS and electron-energy-loss spectroscopy. This corresponds to the maximum film thickness that may be achieved by electron assisted growth.

Figure 7 shows a wide energy range spectrum of an oxide film grown under electron bombardment. The total process time using a current density of 10 μA/cm^2 (100 eV) in 5 $\times10^{-7}$ Torr water vapor is 200 min. The overlayer spectrum

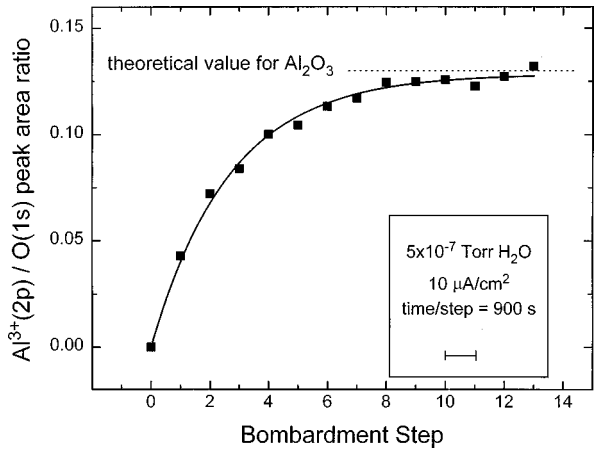

FIG. 6. Al^{3+}($2p$)/O($1s$) peak area ratio as a function of exposure/bombardment. Each step corresponds to 15 min in 5 $\times10^{-7}$ Torr water atmosphere and electron bombardment (10 μA/cm^2, 100 eV). With time the peak area ratio approaches the theoretical value which is expected for an Al_2O_3 stoichiometry with the excitation source and electron energy analyzer employed.

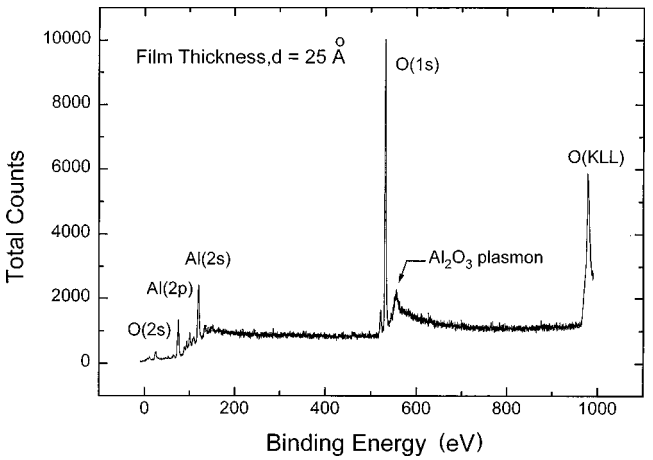

FIG. 7. Wide-range Al $K\alpha$ excited photoelectron spectrum of a 25-Å-thick oxide film grown using electron bombardment. The spectrum only contains oxygen, aluminum and plasmon excitation related loss features with their combinational losses. Starting at low binding energies the main components are the O($2s$) region, the Al($2p$), and Al($2s$) core-level emission with plasmon losses towards higher binding energies, the O($1s$) core-level emission with an aluminum oxide plasmon loss, and the O-(*KLL*) Auger transition.

is essentially identical with tabulated spectra for aluminum oxide and sapphire.[11] Beginning at low binding energies the O($2s$) feature is followed by the Al($2p$) and Al($2s$) core-level region in which are also exhibited plasmon-loss features. An Al(*KLL*) Auger transition (1396 eV kinetic electron energy) is also seen. At about 530 eV binding energy, the dominant O($1s$) peak is seen (the sensitivity of XPS for oxygen is five times larger than for aluminum) together with an aluminum oxide plasmon loss. Finally close to 1 keV binding energy, the O(*KLL*) Auger transition appears. Evaluation of the peak area ratio between the Al^{3+}($2p$) and O($1s$) component (using sensitivity factors from the Leybold-Heraeus compilation) shows that this thick film has the proper Al_2O_3 stoichiometry (the change of apparent stoichiometry during film growth is shown in Fig. 6).

The determination of the film thickness using XPS intensity ratios depends upon the morphology of the aluminum oxide layer, since the signal attenuation differs for an island-like and a homogeneous oxide film on the aluminum substrate. Figure 8 shows the peak area ratio $I(Al^0)/I(Al^{3+})$ of the two XPS Al($2p$) contributions as a function of the photoelectron takeoff angle θ measured from the crystal normal (see inset to Fig. 8). These measurements were made on the same film as in Fig. 7.

If the Al_2O_3 film covers the surface homogeneously the formula

$$\left[\frac{I(Al^0)}{I(Al^{3+})}=\frac{\rho_{Al}}{\rho_{Al_2O_3}}\frac{M_{Al_2O_3}}{2M_{Al}}\frac{\exp[-d/\lambda\,\cos\theta]}{1-\exp[-d/\lambda\,\cos\theta]}\right] \quad (2)$$

should hold. Herein λ denotes the mean free path of x-ray excited core-level electrons, which is 20 Å to good approximation for Al^0 and Al^{3+} in bulk aluminum and aluminum oxide.[18] The parameters ρ_{Al} and $\rho_{Al_2O_3}$ are bulk densities, and M is the molecular weight. It is assumed that the pho-

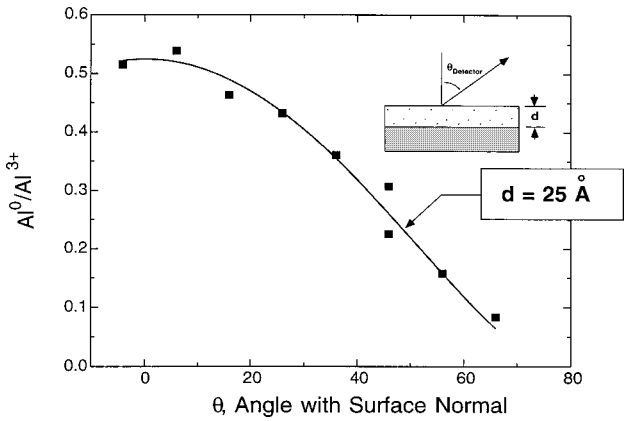

FIG. 8. Al^0/Al^{3+} peak area ratio of the two spectral components of the aluminum core-level emission plotted as a function of the takeoff angle θ. The variation in the Al^0/Al^{+3} ratio can be described by a homogenous Al_2O_3 film of thickness 25 Å on top of the aluminum bulk metal.

toelectron emission cross section for Al does not differ in Al and in Al_2O_3. As can be seen from the solid line in Fig. 8 the signal change with variation of θ can be well described with Eq. (2) using $d=25$ Å. We therefore conclude that the morphology of the Al_2O_3 film grown in water vapor under electron bombardment is most likely to be a homogeneous stoichiometric Al_2O_3 film on top of the aluminum metal substrate.

It follows from Eq. (2) that the oxide thickness d is given by[19]

$$d=\lambda\ \cos\theta\ \ln\left[1+\frac{\rho_{\mathrm{Al}}}{\rho_{\mathrm{Al_2O_3}}}\frac{M_{\mathrm{Al_2O_3}}}{2M_{\mathrm{Al}}}\frac{I(\mathrm{Al}^{3+})}{I(\mathrm{Al}^{0})}\right]. \qquad (3)$$

This relationship was used to establish the thickness scale in Fig. 4.

2. Electronic properties of the thick Al_2O_3 film

Figure 9 shows the electron-energy-loss spectrum of aluminum oxide films grown using comparable water vapor exposures with and without electron bombardment. The energy of the primary electron beam for excitation is 460 eV in both cases. The upper spectrum from the water oxidation still contains the aluminum metal surface plasmon loss at 10.9 eV loss energy, indicating that bare surface areas exist. This is in agreement with previous publications on this system, in which an island growth model for oxidation in a water atmosphere has been favored[17] as has been found also for oxidation in oxygen gas.[20] The most prominent electron energy loss feature in Fig. 9 is the 15.7 eV aluminum bulk plasmon, $\omega_b(\mathrm{Al})$, and its overtones at 31.4 and 46.9 eV. Low-intensity combinational losses of bulk and surface plasmons (ω_b) are also barely visible. The lower spectrum, taken after surface oxidation using electron bombardment, is almost identical with spectra obtained from sapphire surfaces[21] and clearly indicates heavy surface oxidation. The dominating loss feature is the characteristic aluminum oxide plasmonlike loss, $\omega_b(Al_2O_3)$, at 23.5 eV. Furthermore, there is a shoulder at about 15 eV loss energy which might be interpreted as a remaining contribution of an Al bulk plasmon. However, the

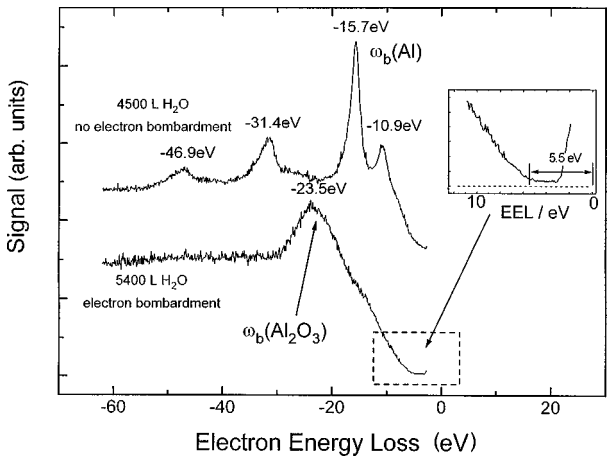

FIG. 9. Electron-energy-loss spectrum (460 eV primary energy) from comparable water exposures with and without electron bombardment. The upper spectrum taken after 4500 L water exposure without electron bombardment contains only aluminum bulk and surface plasmon losses. It is composed of the 10.9 eV surface plasmon and the 15.7 eV bulk plasmon loss and their overtones. The lower spectrum taken after using electron bombardment (10 μA/cm^2, 100 eV) shows only the aluminum oxide plasmon loss at 23.5 eV. Furthermore a band gap of about 5.5 eV (see inset) appears, showing the insulating property of the resulting film.

very same spectrum is observed from sapphire samples[20] indicating that this feature might be an intrinsic property of bulk Al_2O_3. The intensity in the low-energy-loss region is strongly reduced, indicating a band gap of about 5.5 eV width (see inset, Fig. 9), which is characteristic for an insulating material such as aluminum oxide. The observed magnitude of the gap width corresponds well to gap energies measured on sapphire by the same technique.[21]

IV. DISCUSSION

A. Summary of experimental findings

The experimental findings described in Sec. III are as follows.

(1) The O(1s) peak area obtained during oxidation in water vapor increases much faster when bombarding the surface with 100 eV electrons. After comparable exposure times, a strong $Al^{3+}(2p)$ peak has developed using the electron beam, while without bombardment only a small contribution of this feature can be observed for comparable water vapor exposures.

(2) The peak area ratio of $Al^{3+}(2p)/O(1s)$ after reaching saturation thickness is the same as expected from a stoichiometric Al_2O_3 layer. The variation of the peak area ratio $Al^0(2p)/Al^{3+}(2p)$ at various electron emission angles can be described by assuming a homogenous aluminum oxide (Al_2O_3) film with a thickness of 25 Å on top of an aluminum metal substrate. The electron-energy-loss spectrum obtained from this film is very similar to spectra published for sapphire surfaces with an oxide bulk plasmon at 23.5 eV loss energy and a band gap of 5.5 eV.

(3) The $Al^0(2p)/Al^{3+}(2p)$ peak area ratio, under the assumption of a homogenous oxide layer covering the alumi-

num substrate, shows a linear time-dependent increase in oxide thickness with ongoing electron bombardment/water exposure.

(4) During this growth both the $Al^{3+}(2p)$ and the $O(1s)$ core-level binding energies shift in parallel to lower binding energies.

(5) The $Al^{3+}(2p)/O(1s)$ peak area ratio increases monotonically from zero to the value expected for an Al_2O_3 stoichiometry.

(6) The film growth rate abruptly decreases after reaching a thickness of about 25 Å. This approximately coincides with reaching the asymptotic limit of the $Al^{3+}(2p)/O(1s)$ peak area ratio corresponding to the stoichiometry characteristic of Al_2O_3. For longer electron-beam-enhanced oxidation times, no significant growth in thickness and change in peak position is obtained.

From these findings we first of all draw the following conclusions.

(1) Electron bombardment of an aluminum surface in water vapor at room temperature leads to the efficient production of a stoichiometric aluminum oxide film.

(2) The oxide film grows much faster using electron bombardment, compared to growth at 300 K in water vapor alone.

(3) The thickness under our experimental conditions, however, does not exceed the value obtained after extensive thermal oxidation in water vapor without electron bombardment (not shown). After reaching about 25 Å film thickness, film growth virtually stops.

(4) The surface oxidation is accompanied by two main features, which differ from the behavior observed without electron irradiation: (a) The film grows linearly with time instead of obeying a parabolic rate law found for thermally activated oxidation; and (b) The $Al^{3+}(2p)$ and $O(1s)$ core levels shift in parallel to lower binding energies as the electron-beam-assisted oxidation occurs.

B. Brief summary of previous studies of thermal and electron-beam-assisted oxidation of aluminum

At room temperature, water dissociates on both a clean and an oxygen-covered aluminum surface.[22,23] The surface is covered with -OH groups that are stable up to nearly 700 K. This thermally activated dissociation process is quenched at 90 K, and water exists as an undissociated ice film on Al(111).[5] However, a thin ice film can be efficiently activated by 100 eV electron impact, converting the surface to Al_2O_3 with a high efficiency corresponding to a high cross section of 2.5×10^{-16} cm^2.[5] In the studies reported here at 300 K, either adsorbed H_2O in a transient state which exists prior to dissociation, and/or adsorbed -OH species act as a source of the oxidizing species upon electronic excitation by 100 eV electrons. The low gas density of H_2O in the growth experiments excludes H_2O excitation in the gas phase by electron impact.

C. Mechanism of Al_2O_3 film formation—thermally activated process

The theory for thermally activated thin film formation ($d\leqslant100$ Å) was first described by Cabrera and Mott in 1948.[24] The driving force in this thickness regime is the electric field set up by negative oxygen ions on the oxide outer surface. This field either draws metal cations to the surface or leads to the migration of oxygen anions to the metal/insulator interface. The charge transfer due to ion migration has to be balanced by an electron flux from the metal substrate towards the oxide surface to maintain change neutrality. Since the insulating oxide layer is sufficiently thin, enough electrons can pass into the film by tunneling to keep the oxide growth process going. The thermally activated growth rate is considered to be limited by the ion mobility. However, different views have been published.[25]

We propose that the electron bombardment of the hydrated oxide surface leads by means of electron-impact induced chemical reaction[5] to a higher concentration of oxygen anions on the oxide surface and in this way increases the oxidation rate. We will present evidence for this interpretation below.

Usually in thermally activated oxidation, it is assumed that the potential drop ΔV across the film is constant during the growth process. Thus as the film thickness increases, the electric field in the oxide layer decreases. In this case, the potential drop is determined by the position of the electron affinity level in the oxide relative to the bulk Fermi level in the metal. Electrons tunnel through the film populating the affinity level, creating oxygen ions until a potential difference is set up by the resulting charge accumulation on the oxide surface that shifts the affinity level to the Fermi level and terminates the electron flux. The growth of the oxide film, which depends on the individual mobilities, proceeds via the transport of metal and/or oxygen ions through the oxide film. In case of Al_2O_3 strong evidence has been reported that dominantly oxygen ions migrate.[26] The corresponding particle current density j is given by

$$j=\mu nE-D\frac{dn}{dx} \tag{4}$$

with μ being the mobility of the diffusing ion species, n the density of ions, and D the ion diffusion coefficient. For thin films the effect of the electric field E dominates in the ion transport process and the term in Eq. (4) containing the concentration gradient, dn/dx, can be neglected.

Assuming a capacitorlike behavior of the metal/oxide structure with a constant potential drop ΔV across its thickness, the electric field driving the ionic motion in thermally activated oxidation then decreases with increasing film thickness x so that $E=\Delta V/x$. Considering the ionic motion being dominated by the field-induced migration, the film thickness changes so that $dx/dt\propto\Delta V/x$, and a parabolic growth kinetic law ($x\propto t^{1/2}$) is observed for the thermally activated oxidation process.

D. Mechanism of Al_2O_3 film formation—electron-beam-assisted oxidation

The growth law observed in our study of an electron-impact-activated oxidation process differs significantly from the expected parabolic kinetic film-growth behavior. Electron bombardment of the oxide surface in water vapor gives a constant growth rate up to a limiting thickness as shown in Fig. 4. Keeping with the Cabrera-Mott field-induced oxide

growth picture, this behavior corresponds to the presence of a *constant* electric field during the growth phase, caused by a *constant* surface coverage of anions at the oxide surface. This interpretation is confirmed by the observed parallel shifts of the $Al^{3+}(2p)$ and $O(1s)$ core-level emission peaks with increasing film thickness. Since both peaks shift in parallel in the same direction (see Fig. 5), this shift is not caused by a change in the chemical film composition (like aluminum hydroxide converting with time into aluminum oxide or vice versa). Moreover, we can remove the $Al^{3+}(2p)$ and $O(1s)$ peak shift by heating to 473 K and can then recover the shift by electron bombardment without water exposure afterwards (not shown). Therefore, we interpret the observed peak shifts as being due to the accumulation of surface charge as a result of electron bombardment. The direction of the shift towards increasing electron kinetic energies shows that the sign of this stored charge on the outer oxide surface is negative. The $O(1s)$ shift towards lower binding energy upon increasing oxide thickness has been observed before and attributed to charge accumulation as well during thermally activated oxidation.[26] X-ray photoelectron spectroscopy is well suited to investigate electrostatic potential differences in thin semiconducting and insulating films.[27–29]

Next we have to consider how charge might be stored in the growing oxide film. Since electrons can be regarded as highly mobile as mentioned above, one would assume that any charge accumulation due to electrons would dissipate rather quickly. Therefore, we propose that the negative charge is in the form of oxygen ions on the oxide surface in the way described by the Cabrera-Mott oxide growth model. This interpretation is confirmed by considering another effect of the electron and x-ray bombardment. At 100 eV primary beam energy as well as under x-ray bombardment, we observe a positive sample current towards ground, i.e., more secondary electrons leave the sample than primary electrons are injected. Therefore, if charge storage due to the balance of electron arrival and emission occurs in the film, it should have a positive rather than a negative sign and the core-level peak shifts should be in the opposite direction. If, however, the primary way to accumulate charge is the formation of oxygen ions on the film surface, necessarily the observed core-level shift to higher kinetic energies will occur.

If this interpretation is correct the peak shifts should follow from a simple model by again assuming a surface capacitor consisting of a grounded plate (the substrate), a dielectric filling layer (the oxide film), and a negatively charged second plate (oxygen ions on the oxide surface). Figure 10 sketches this situation that is identical to the model from the Cabrera-Mott theory for thermal oxidation. Indeed the magnitude of the shifts of both peaks can be described by assuming a linear potential drop between the oxide surface and the metal/oxide interface with a *constant* electric field of 5×10^6 V/cm in the oxide film independent of film thickness. This condition follows from a *constant* anion charge density on the oxide film surface during electron bombardment. The solid lines in Fig. 5 show the result of the calculation taking the finite elastic mean free path of 20 Å for electrons from the $Al(2p)$ level and 15 Å for electrons from the $O(1s)$ level into account. As can be seen the resulting curves fit the data well.

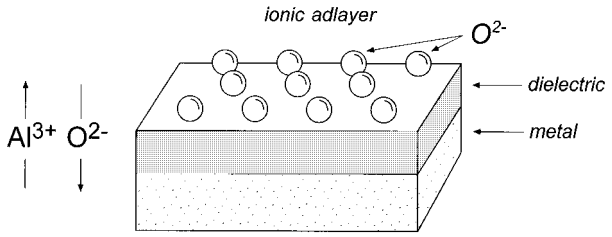

FIG. 10. Thin film growth according to the Cabrera-Mott mechanism (Ref. 24). Oxygen ions, produced by electron-impact induced chemistry involving H_2O on the surface, lead to a strong electric field in the oxide layer that drives ionic migration through the film. Depending on the specific mobilities, either Al^{3+} ions move towards the oxide surface or oxygen ions towards the metal/oxide interface. The transport of electrons is considered to be independent of the ionic motion and fast in comparison.

This electric-field strength is rather high and of the order of the breakthrough field for aluminum oxide films, which is in the range $(3-13)\times10^6$ V/cm.[30] Most likely the amount of surface charge is limited by the dielectric strength of the oxide material and electron bombardment and breakthrough discharging stabilize the field at an equilibrium value.

Assuming a dielectric constant $\varepsilon=10$ independent of film thickness corresponding to a constant film composition, the surface charge density σ can be calculated by

$$\sigma=\varepsilon\varepsilon_0 E=\varepsilon\varepsilon_0\Delta V/x. \tag{5}$$

Assuming the formation of O^{2-} ions this density corresponds to a density of oxygen ions of 1.4×10^{13} O^{2-}/cm^2, and a nearest-neighbor distance of 29 Å if the oxygen ions form a hexagonal lattice. The binding energy per ion can be approximated by classical electrodynamics, assuming regularly arranged point charges in front of a dielectric layer on top of a grounded metal substrate. With a distance of 3 Å between point charge and surface of the dielectric (the oxygen ion radius is 1.4 Å in ionic crystals), a nearest-neighbor distance of 30 Å in the ion lattice and an oxide thickness of 30 Å with dielectric constant $\varepsilon=10$ the binding energy per oxygen ion is 1.6 eV. This number takes the attractive interaction with the image charges and the repulsive interaction within the oxygen ion lattice into account. While this simple model is certainly a crude picture of the true charge arrangement and the surface electronic structure, the estimated anion binding energy nevertheless shows that despite the accumulated charge density, the ion layer is well stabilized and our picture of the charge location is reasonable. A constant density of oxygen ions on the oxide surface results in a normal electric field E independent of film thickness, and a constant flux of ions through the oxide film. Therefore an oxide growth rate which is linear in time is obtained.

Interestingly we observe a drop in film growth rate at about 25 Å film thickness. The uptake either completely terminates or slows down by an order of magnitude. The obtained thickness limit is the same as found when thermally oxidizing the aluminum surface in air, oxygen or water atmosphere.[24,20,32] The natural growth of an oxide film in a gaseous or liquid environment, in principle, is limited by the decreasing growth rate with increasing film thickness. This is true for the thin film region, where the Cabrera-Mott model holds, as well as for higher thickness, where different ion

transport mechanisms have to be considered.[24] Stimulating the formation of surface oxygen ions by electron bombardment does not lead to unlimited oxidation as well. Because of energetic and kinetic reasons the oxidation process will come to an end.

Considering the interaction of oxygen ions on the surface on the basis of classical electrodynamics it is evident that the interionic repulsion will exceed the attraction by the image charges beyond a certain film thickness because of the finite dielectric constant of the oxide film. Therefore, for each oxide thickness d there is a maximum density $\sigma_{\max}(d)$ of oxygen ions, which can be bound to the insulator-on-metal system. This maximum density decreases monotonically with increasing film thickness. Therefore, even if one can supply sufficient charge to the surface or activate the ion formation sufficiently by electron bombardment, the electric field as the driving force for ion migration will decrease due to a naturally decreasing charge density on the oxide surface. How close the actual charge density comes to the limit $\sigma_{\max}(d)$ is determined by the balance between ion formation rate I and the rate of ion migration M:

$$\frac{d\sigma}{dt} = I(\sigma) - M(\sigma)$$

(possibly mechanisms other than ion migration for decreasing the surface charge density have to be considered in addition). In principle, both rates might depend on the charge density itself. In a simple model the ion formation rate might just be given by the electron bombardment rate and therefore be independent of σ. The ion migration rate might be proportional to the magnitude of the electric field E and, therefore, be proportional to the charge density as well:

$$M(\sigma) = \tilde{M}\sigma.$$

This would lead to a steady-state charge density σ_{ss} of

$$\sigma_{\mathrm{ss}} = \frac{1}{\tilde{M}},$$

which is independent of film thickness until the film reaches the point where

$$\sigma_{\mathrm{ss}} = \sigma_{\max}(d).$$

From then on the charge density on the surface would decrease with growing film thickness, resulting in a decreasing growth rate starting from this point. In this case the shift of the Al($2p$) and O($1s$) core-level emission should reflect the decreasing electric field in the oxide film by a decrease in slope of the $\Delta E(d)$ curve (see Fig. 5), which is not observed experimentally over most of the range. Instead of for energetic reasons, the film growth might also terminate because of a change in the growth kinetics. If, for example, the migration of ions across the film is considerably hindered above a certain thickness, then the growth rate will decrease as well, since less ions per unit time cross the insulator layer. Such an effect might arise if the ionic migration leads over certain paths like grain boundaries or other defect sites, which decrease in number when the film grows thicker.

If diffusion along defect sites is the favorable path for ion migration, the growth rate will slow down once the number of these defect sites decreases. Diffusion of oxygen ions toward the surface along grain boundaries is considered to be the dominant transport process at least for high-temperature oxidation.[33] If the oxide growth proceeds as in the case of molecular oxygen in the form of isolated islands which interlink after reaching a thickness of about 20 Å,[20] then one could very well imagine a decrease in film growth rate as we observe; since interlinking of these oxide grains could turn off the oxygen ion flux by removal of their favorable migration path along surfaces.

This effect would be expected to result in an increase in E near the end of the film growth process as a result of an increase in steady-state charge density σ_{ss} and this is indeed observed in Fig. 5 near the termination of rapid film growth.

Below the saturation coverage an excess of O($1s$) signal compared to the proper intensity ratio for Al_2O_3 is observed. This might be due to hydroxyl group coverage on Al_2O_3 cluster surfaces. Reaching saturation thickness coincides with saturation of the $Al^{+3}(2p)/O(1s)$ ratio at a value corresponding to Al_2O_3 stoichiometry, and the removal of the majority of surface hydroxyl groups from the cluster surfaces as clusters coalesce.

V. CONCLUSIONS

The oxidation rate of an Al(111) surface in water vapor can be significantly increased by electron bombardment of the surface with 100 eV electrons at a current density of 10 μA/cm^2. The resulting amorphous aluminum oxide film, with a limiting thickness of about 25 Å, has the correct Al_2O_3 stoichiometry and covers the aluminum substrate homogeneously as determined by XPS. The electronic properties of the produced film are qualitatively the same as obtained from a sapphire surface, exhibiting the oxide plasmon at 23.5 eV loss energy and with a band gap of about 5.5 eV.

The observed oxygen uptake and core-level peak shifts can be interpreted on the basis of the Cabrera-Mott model of thin film growth, assuming the electric field within the oxide layer is caused by oxygen anions on the oxide surface as the driving force for ion migration. The increase in growth rate under electron bombardment is caused by electron-beam-induced dissociation of adsorbed water molecules and enhanced surface oxygen anion formation. Due to the electron bombardment the surface coverage of oxygen anions and accordingly the electric field within the oxide layer is kept constant at about 5×10^6 V/cm and does not depend on the thickness of the film. Therefore, the transport of ions through the film is independent of thickness as well, and the growth rate is constant and independent of time. Even though the electric field within the layer does not break down, the growth terminates when a saturation thickness of about 25 Å is reached. We interpret the abrupt drop in film growth rate at this point as being due to a change in the ion-transport mechanism. Most likely the ions migrate preferentially along defect sites such as grain boundary borders or through only partially oxidized regions. Once the film heals out these paths by Al_2O_3 cluster coalescence, these paths are no longer

available and the oxidation rate decreases significantly. Accordingly, we observe the film to reach the Al_2O_3 stoichiometry in coincidence with the stop in film growth.

A useful application of our study might be the controlled growth of aluminum oxide films over extended areas by using a low-energy electron beam, or possibly in a more localized application by using the tunneling of electrons between an STM tip and the substrate. Finally the modification of the surface oxygen ion density by electron bombardment might supply new ways to control the growth of thin oxide films at low temperatures.

ACKNOWLEDGMENT

The full support of the Air Force Office of Scientific Research (AFOSR) is gratefully acknowledged.

[1] C. E. Melton, J. Chem. Phys. **57**, 4218 (1972).
[2] M. Jungen, J. Vogt, and K. Staemmler, Chem. Phys. **37**, 49 (1979).
[3] D. Klyachko, P. Rowntree, and L. Sanche, Surf. Sci. **346**, L49 (1996).
[4] R. Martel, Ph. Avouris, and I. W. Lyo, Science **272**, 385 (1996).
[5] H. D. Ebinger and J. T. Yates, Jr., Surf. Sci. (to be published).
[6] J. W. Park and A. J. Pedraza, J. Vac. Sci. Technol. A **14**, 286 (1996).
[7] A. Hoffmann and P. J. K. Paterson, Surf. Sci. **352**, 993 (1996).
[8] V. Smentkowski, H. Jänsch, M. A. Henderson, and J. T. Yates, Jr., Surf. Sci. **330**, 207 (1995).
[9] M. J. Bozack, L. Muehlhoff, J. N. Russell, Jr., W. J. Choyke, and J. T. Yates, Jr., J. Vac. Sci. Technol. A **5**, 1 (1987).
[10] A. Winkler and J. T. Yates, Jr., J. Vac. Sci. Technol. A **6**, 2929 (1988).
[11] C. D. Wagner, W. M. Riggs, L. E. Davis, J. F. Moulder, and G. E. Muilenberg, *Handbook of X-ray Photoelectron Spectroscopy* (Perkin Elmer, Eden Prairie, MN, 1979); M. Gautier, J. P. Durand, L. Pham, and M. J. Guittet, Surf. Sci. **250**, 71 (1991).
[12] T. W. Barefoot, H. D. Ebinger, and J. T. Yates, Jr., J. Vac. Sci. Technol. A **15**, 2740 (1997).
[13] A. Jimenez-Gonzalez and D. Schmeisser, Surf. Sci. **250**, 59 (1991).
[14] S. A. Flodstrom, R. Z. Bachrach, R. S. Bauer, and S. B. Hagström, Phys. Rev. Lett. **37**, 1282 (1976).
[15] A. Arranz and C. Palacio, Surf. Sci. **355**, 203 (1996).
[16] P. M. A. Sherwood, in *Practical Surface Analysis*, edited by D. Briggs and M. P. Seah (Wiley, New York, 1983).
[17] W. H. Krueger and S. R. Pollack, Surf. Sci. **30**, 280 (1972).
[18] M. P. Seah and W. A. Dench, Surf. Interface Anal. **1**, 2 (1979).
[19] G. Ertl and J. Küppers, *Low Energy Electrons and Surface Chemistry* (VCH, Weinheim, 1985).
[20] H. Brune, J. Wintterlin, J. Trost, G. Ertl, J. Wiechers, and R. J. Behm, J. Chem. Phys. **99**, 2128 (1993).
[21] M. A. Schildbach and A. V. Hamza, Surf. Sci. **282**, 306 (1993).
[22] F. P. Netzer and T. E. Madey, Surf. Sci. **127**, L102 (1983).
[23] J. E. Crowell, J. G. Chen, D. M. Hercules, and J. T. Yates, Jr., J. Chem. Phys. **86**, 5804 (1987).
[24] N. Cabrera and N. F. Mott, Rep. Prog. Phys. **12**, 163 (1948).
[25] B. Ya Moizhes, Fiz. Tverd. Tela (Leningrad) **26**, 576 (1984) [Sov. Phys. Solid State **26**, 347 (1984)].
[26] C. Ocal, S. Ferrer, and N. Garcia, Surf. Sci. **163**, 335 (1985).
[27] W. M. Lau, J. Appl. Phys. **65**, 2047 (1989).
[28] W. M. Lau, J. Appl. Phys. **67**, 1504 (1990).
[29] R. W. Kwok, W. M. Lau, D. Landheer, and S. Ingrey, J. Electron Microsc. **22**, 1141 (1993).
[30] N. Klein and M. Albert, J. Appl. Phys. **53**, 5840 (1982).
[31] A. Bianconi, R. Z. Bachrach, S. B. M. Hagström, and S. A. Flodström, Phys. Rev. B **19**, 2837 (1979).
[32] We find this oxide thickness after exposing the aluminum crystal to the atmosphere.
[33] A. Atkinson, Rev. Mod. Phys. **57**, 437 (1985).